Geophysical Journal International

Geophys. J. Int. (2011) **185,** 1175–1188 doi: 10.1111/j.1365-246X.2011.05022.x

$^{40}Ar/^{39}Ar$ dating of Quaternary lavas in northwest Iran: constraints on the landscape evolution and incision rates of the Turkish–Iranian plateau

Mark B. Allen,[1] Darren F. Mark,[2] Monireh Kheirkhah,[3] Dan Barfod,[2] Mohammad H. Emami[3] and Christopher Saville[1]

[1]*Department of Earth Sciences, University of Durham, Durham,* DH1 3LE*, UK. E-mail: m.b.allen@durham.ac.uk*
[2]*NERC Argon Isotope Facility, Scottish Universities Environmental Research Centre, East Kilbride,* G75 0QF*, UK*
[3]*Research Institute for Earth Sciences, Geological Survey of Iran, Azadi Square, Meraj Avenue, Tehran, Iran*

Accepted 2011 March 17. Received 2011 March 15; in original form 2011 January 21

SUMMARY

We report five new $^{40}Ar/^{39}Ar$ ages for basaltic lavas in the Maku region of northwest Iran, between *ca.* 1.87 and 0.40 Ma, which help constrain the tectonic and landscape evolution of this part of the Turkish–Iranian plateau. Flows originated from the composite volcanoes Ararat (Agri Dagi), Tendürek and Yigit Dagi, in eastern Turkey (Anatolia). These volcanoes are within the Turkish–Iranian plateau, which is a consequence of the Arabia–Eurasia collision, but has a poorly constrained evolution and surface uplift history. Current plateau elevations are typically 1.5–2 km, and relief between non-volcanic summits and basins is typically on the scale of ∼1 km. Samples are from flows that passed along pre-existing river valleys. Gorges were cut by re-established rivers after the eruptions, but the great majority of the local relief (∼95 per cent) lies above the sampled flows and so most likely pre-dates the volcanism. Gorge depths and lava ages allow local Quaternary fluvial incision rates to be calculated, which are ∼0.01 to 0.05 mm yr^{-1}. These rates imply slow surface uplift of this part of the Turkish–Iranian plateau during the Quaternary. We therefore constrain the generation of the great majority of relief in the study area to be pre-Quaternary, and caused by the tectonic construction of the plateau, rather than a subcrustal origin related to the Quaternary magmatism.

Key words: Continental neotectonics; Tectonics and landscape evolution; Asia.

1 INTRODUCTION AND GEOLOGICAL SETTING

In this paper we explore the relationships between tectonics, magmatism and landscape evolution in the Turkish–Iranian plateau, northwest Iran, to understand better the development of such orogenic plateaux in general.

Orogenic plateaux are constructed as a result of subduction at convergent continental margins or continent–continent collision. The Tibetan and Turkish–Iranian plateaux are formed by the India–Eurasia and Arabia–Eurasia collisions, respectively (Hatzfeld & Molnar 2010), and are first-order geomorphic features of the Eurasian landscape. However their tectonic evolution and surface uplift history are not clearly understood, even though there may be consequences for climate on regional if not global levels (Raymo *et al.* 1988; Molnar *et al.* 2010). This paper presents new $^{40}Ar/^{39}Ar$ ages for lavas in the Maku region of northwest Iran (Figs 1 and 2), within the Turkish–Iranian plateau. The sampled lavas have an unusual setting: they travelled through pre-existing river valleys for tens of kilometres. After eruption, the valleys were reoccupied by the present rivers, which have cut gorges on the scale of 10–50 m through the lavas. Therefore the $^{40}Ar/^{39}Ar$ ages allow determination of fluvial incision rates at the sample sites, and help constrain the landscape evolution of this part of the Turkish–Iranian plateau, before and after the eruptions. Such information is valuable not only because it explains why the development of topographic relief, but because this evolution relates directly back to tectonic, climatic and magmatic processes that operate on geological timescales.

However, it is typically difficult to obtain information on the generation of relief because we lack the tools and natural laboratories on which to work. Thermochronology provides valuable information about denudation rates, but this is distinct from surface uplift and only provides information on relief generation in unusual circumstances or specific modelling and sampling strategies (Valla *et al.* 2010; Van Der Beek *et al.* 2010). Combined bedrock thermochronometry and $^{40}Ar/^{39}Ar$ ages for incised lavas were used by Schildgen *et al.* (2007) to understand the topographic evolution of the western margin of the Andean plateau. Here, interfluve erosion rates are both known and slow, thereby allowing relatively simple conversion of incision rates in to surface uplift rates.

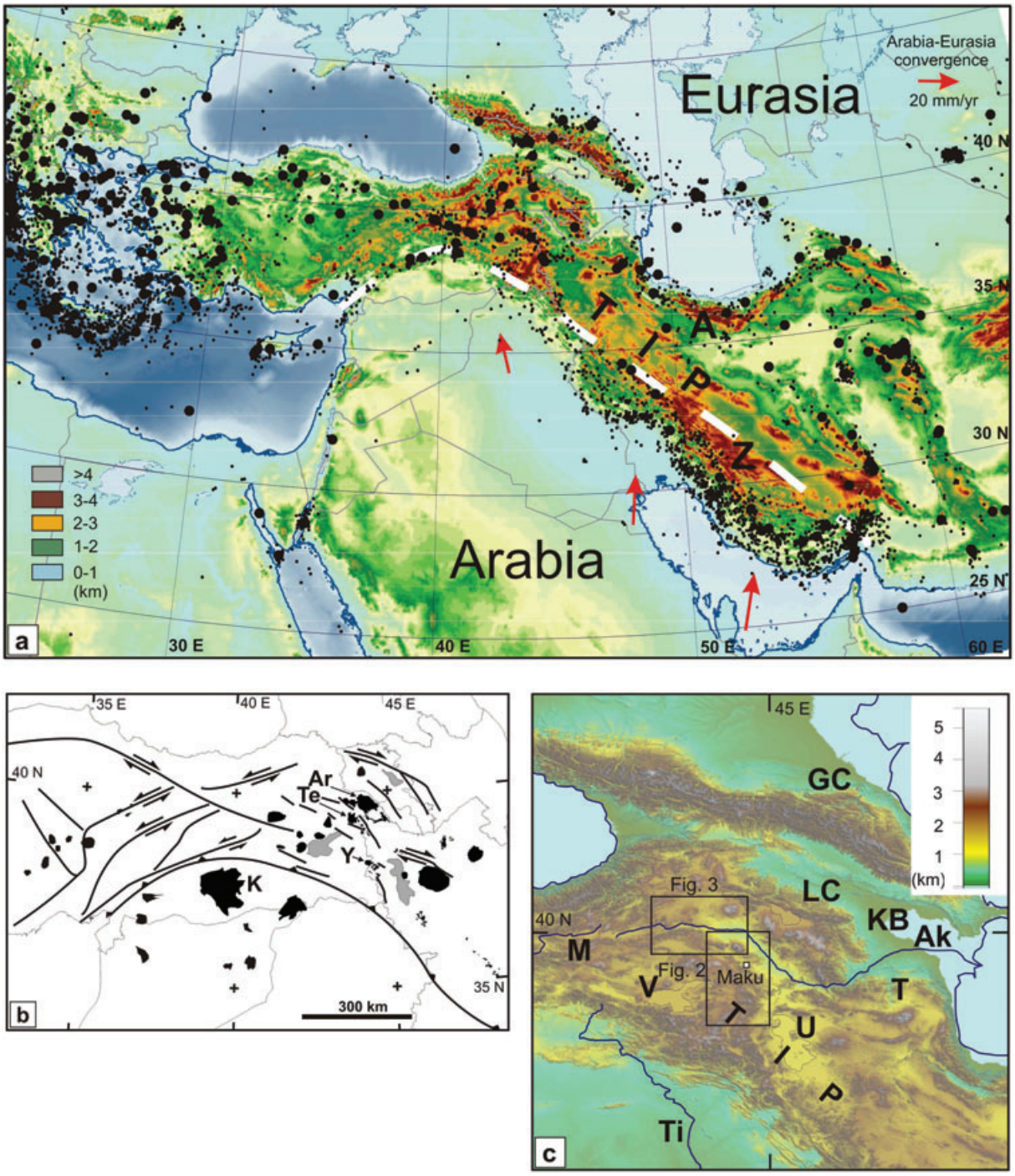

Figure 1. (a) Regional topography and seismicity of the Arabia–Eurasia collision. Large dots are epicentres of earthquakes of $M > 6$ from 1900 to 2000 (Jackson 2001), small dots are epicentres from the EHB catalogue 1964–1999, $M > \sim 5$. Red arrows show GPS-derived velocity with respect to Asia from Sella *et al.* (2002), A, Alborz; TIP, Turkish–Iranian plateau; Z, Zagros. (b) Location of late Cenozoic, largely Quaternary volcanic centres in eastern Anatolia and northwest Iran (black). Grey areas are lakes Van, Urumieh and Sevan. From Kheirkhah *et al*. (2009) and sources therein. Ar, Ararat; K, Karacalidag; Te, Tendürek; Y, Yigit Dagi. (c) Topography of eastern Anatolia and northwest Iran, derived from SRTM data. Ak, Araks River; GC, Greater Caucasus; LC, Lesser Caucasus; KB, Kura Basin; M, Murat; T, Talysh; Ti, Tigris; TIP, Turkish–Iranian plateau; U, Lake Urumieh; V, Lake Van.

The Turkish–Iranian plateau is a major element of the Arabia–Eurasia collision zone. It covers roughly 1 500 000 km^2, mainly across eastern Turkey and Iran, with elevations typically in the range of 1.5–2 km (Fig. 1a). Basins in eastern Iran are as low as ∼500 m above sea level. Relief within the plateau is subdued compared with mountain ranges at the plateau margins such as the Zagros, Alborz and Caucasus (which all contain non-volcanic peaks >4000 m), but can still be considerable: ridges and summits rise >1 km above adjacent basins. Internal deformation rates within most of the plateau are low, and the (Global Positioning System) GPS-derived velocity field for Iran indicates <2 mm yr^{-1} internal deformation across the Iranian sector of the plateau (Vernant *et al.*

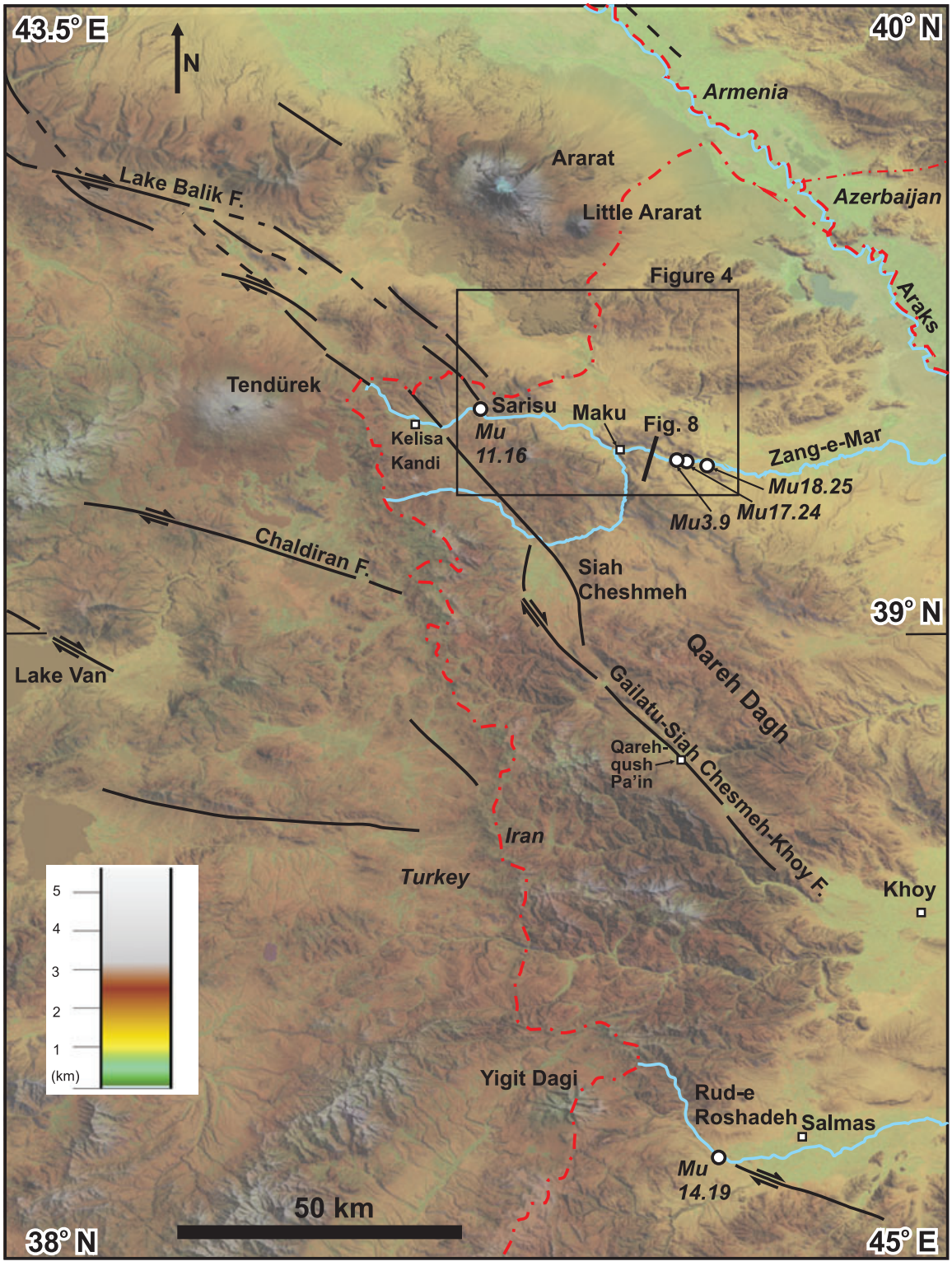

Figure 2. Sample localities and active faults of the Maku region, northwest Iran, derived from Alavi & Bolourchi (1975), Dewey *et al.* (1986), Yilmaz *et al.* (1998) and Copley & Jackson (2006) and our own observations. Background is 50 per cent transparent Landsat 7 imagery draped over SRTM digital topography. Red dashed line = international boundary; blue line = river described in text.

2004). The velocity field for easternmost Turkey and western Iran suggests higher slip rates (Reilinger *et al.* 2006), with up to 8 mm yr^{-1} on individual faults (Copley & Jackson 2006).

In keeping with the GPS data, the seismicity record shows that the plateau undergoes little seismogenic thrusting at present within its interior (Jackson *et al.* 1995; Jackson 2001; Allen *et al.* 2004). Active thrusting is concentrated in the mountain ranges at its margins (Fig. 1a). Lower Miocene limestones within eastern Turkey and central Iran show that at least large parts of these areas were under sea level until as late as ~20–16 Ma (Şenel 2002; Reuter

et al. 2009). These rocks are regionally folded, indicating a degree of late Cenozoic crustal shortening and thickening (Morley *et al.* 2009; Ballato *et al.* 2011), which also affected northwest Iran (Alavi & Bolourchi 1975). There are few constraints on the timing of deformation within this broad temporal framework.

Available data on crustal and lithospheric thicknesses indicate a heterogeneous structure beneath the plateau. Crustal thickness estimates based on seismic receiver function analysis are 42 ± 2 km across Central Iran (Paul *et al.* 2010), and 38–53 km within northwest Iran (Taghizadeh-Farahmand *et al.* 2010), which is considerably less than the suture zone to the south (55–70 km, Paul *et al.* 2010) or the Alborz to the north (up to 58 km, Radjaee *et al.* 2010). Crustal thicknesses under eastern Anatolia are ∼45 km (Angus *et al.* 2006). Maggi & Priestley (2005) used seismic tomography to show low-velocity regions in the mantle beneath the plateau, while Priestley & McKenzie (2006) used variations in *S*-wave velocities to show the presence of a >200-km-thick lithosphere core underlying southwest Iran, including the southern part of the plateau. *P*- and *S*-wave receiver function studies within eastern Anatolia suggest the presence of unusually thin mantle lithosphere under this region (e.g. Zor *et al.* 2003; Angus *et al.* 2006).

Magmatism is an important feature of the Turkish–Iranian orogenic plateau, not only because some of the volcanoes dominate the landscape, but because they demonstrate that mantle conditions are such that melting takes place. Composite volcanoes and lava fields are present from Anatolia to eastern Iran (Fig. 1b, Pearce *et al.* 1990; Keskin *et al.* 1998; Walker *et al.* 2009). Most volcanic centres are located on the Eurasian side of the original suture, that is, above the previous Tethyan subduction zone, although Karacalidag in eastern Turkey lies within the Arabian plate (Pearce *et al.* 1990; Lustrino *et al.* 2010).

Sporadic volcanism occurred across eastern Turkey and Iran in the Oligocene–Miocene, including volcanic centres in eastern Anatolia formed at ∼10 Ma (Keskin *et al.* 1998) or even earlier (Lebedev *et al.* 2010). Many centres within eastern Turkey and Iran are Pliocene-Quaternary in age (Yilmaz *et al.* 1998; Davidson *et al.* 2004; Shabanian *et al.* 2009; Walker *et al.* 2009; Ahmadzadeh *et al.* 2010), and so formed tens of millions of years after initial plate collision, which was as early as 20 Ma (Okay *et al.* 2010) or even 35 Ma (Allen & Armstrong 2008).

The reason for this upsurge in magmatism is not clear, although in places there is a close association between the volcanoes and active fault systems, especially pull-apart basins, fault terminations or boundaries between different fault blocks (Yilmaz *et al.* 1998; Karakhanian *et al.* 2004; Allen *et al.* 2011). Either localized extension provides a trigger for melting directly underlying mantle—which has implications for the connectivity of upper crustal structures with much deeper levels of the lithosphere—or there is regional mantle melting that finds conduits to the surface via such fault systems. Rock types in eastern Anatolia and northwest Iran span the compositional range from primitive basalts to rhyolites, with rare potassic and ultrapotassic lavas (Keskin *et al.* 2006; Kheirkhah *et al.* 2009; Ahmadzadeh *et al.* 2010). Many units possess supra-subduction zone chemistries, presumably inherited from sources influenced by the pre-collision Tethyan subduction, although the signature could be related to the Pan-African creation of juvenile lithosphere (Kheirkhah *et al.* 2009). Alkali basalts with within-plate, ocean island basalt (OIB)-like chemistry are also present, especially along strike-slip fault zones, implying that local tapping of mantle with asthenopsheric characteristics can occur (Parlak *et al.* 2001; Walker *et al.* 2009). The cause of the magmatism is not clear. Various processes have been invoked, including slab break-off and detachment/delamination of the lower lithosphere (Pearce *et al.* 1990; Keskin 2003; Şengör *et al.* 2003; Keskin *et al.* 2006; van Hunen & Allen 2011).

Magmatism apparently post-dates compressional deformation in each local area where it occurs. Damavand volcano, which lies within the actively thrusting Alborz mountains of northern Iran, may be an exception, but even this centre may relate to local oblique extension within the range interior (Ritz *et al.* 2006).

Therefore there is evidence that the rise of the Turkish–Iranian plateau to its present elevation has taken place since ∼16 Ma, which is approximately the age of the last marine sedimentation in many areas. Part of this surface uplift may relate to crustal shortening and thickening, but such deformation does not take place at present in the plateau interior, given the evidence of the seismicity and GPS data sets. It is not well constrained whether the relief and surface uplift of the plateau accompanied the crustal shortening, or is more related to the magmatism that post-dated the shortening. This study helps to provide answers to this problem, by targeting an area where lava flows fortuitously provide a marker of the landscape evolution on a geological timescale.

2 REGIONAL GEOMORPHOLOGY

Mountain ridges in the study area trend NNW–SSE in the south, before changing to a more WNW–ESE orientation to the west of Ararat, roughly parallel to the tectonic boundaries shown in Şengör *et al.* (2008) (Fig. 2). Much of the highest ground has bedrock of Upper Cretaceous mélange (Alavi & Bolourchi 1975). Ridges of Permian and Oligocene–Miocene limestone are also prominent in the landscape.

The regional drainage divide lies close to the political Iran/Turkey border (Fig. 2). Rivers on the western side of the main drainage divide flow westwards in to Lake Van, which is internally drained. Rivers that flow east across northernmost Iran eventually join the Araks River (Fig. 2), which flows from its source in eastern Turkey to the Caspian Sea (Fig. 1c). The longitudinal profile of the Araks has two unusually steep reaches or knickzones that depart from the concave-up profile of idealized graded rivers (Fig. 3a). The lower, eastern one lies at the junction of the Lesser Caucasus and Talysh mountains (Fig. 1c), which is where the Araks leaves the Turkish–Iranian plateau and descends towards the plains of the Kura Basin. The western knickzone lies within eastern Turkey, where the Araks cuts a valley up to ∼1 km deep through the undulating, low-relief landscape of the Kars plateau (Figs 3b and c, topographic profiles X–X′ and Y–Y′). East of the Kars plateau, the Araks flows across a broad floodplain (Fig. 3c, profile Z–Z′), although this region still shows up on the river long profile as part of the knickzone (Fig. 3a).

The lavas in this study are from the composite volcanoes Ararat (Agri Dagi), Tendürek and Yigit Dagi, which dominate the landscape close to the Iran/Turkey border, the highest point being the main summit of Ararat, at 5137 m (Figs 1 and 2). Ararat and Tendürek have their main cones within easternmost Turkey (Ararat is a double centre); Yigit Dagi straddles the border.

Ararat sits south of the Araks River. Streams flowing due south join the Zang-e-Mar at Maku (Fig. 2). Slopes on the south side of Tendürek lie within the Lake Van drainage basin. Rivers rising on the east flanks of Tendürek flow to the Zang-e-Mar. Rivers flowing north join other tributaries of the Murat and eventually join the Euphrates, or become ponded in the land between Tendürek and Ararat. Yigit Dagi lies to the south of Tendürek and Ararat. It sits at

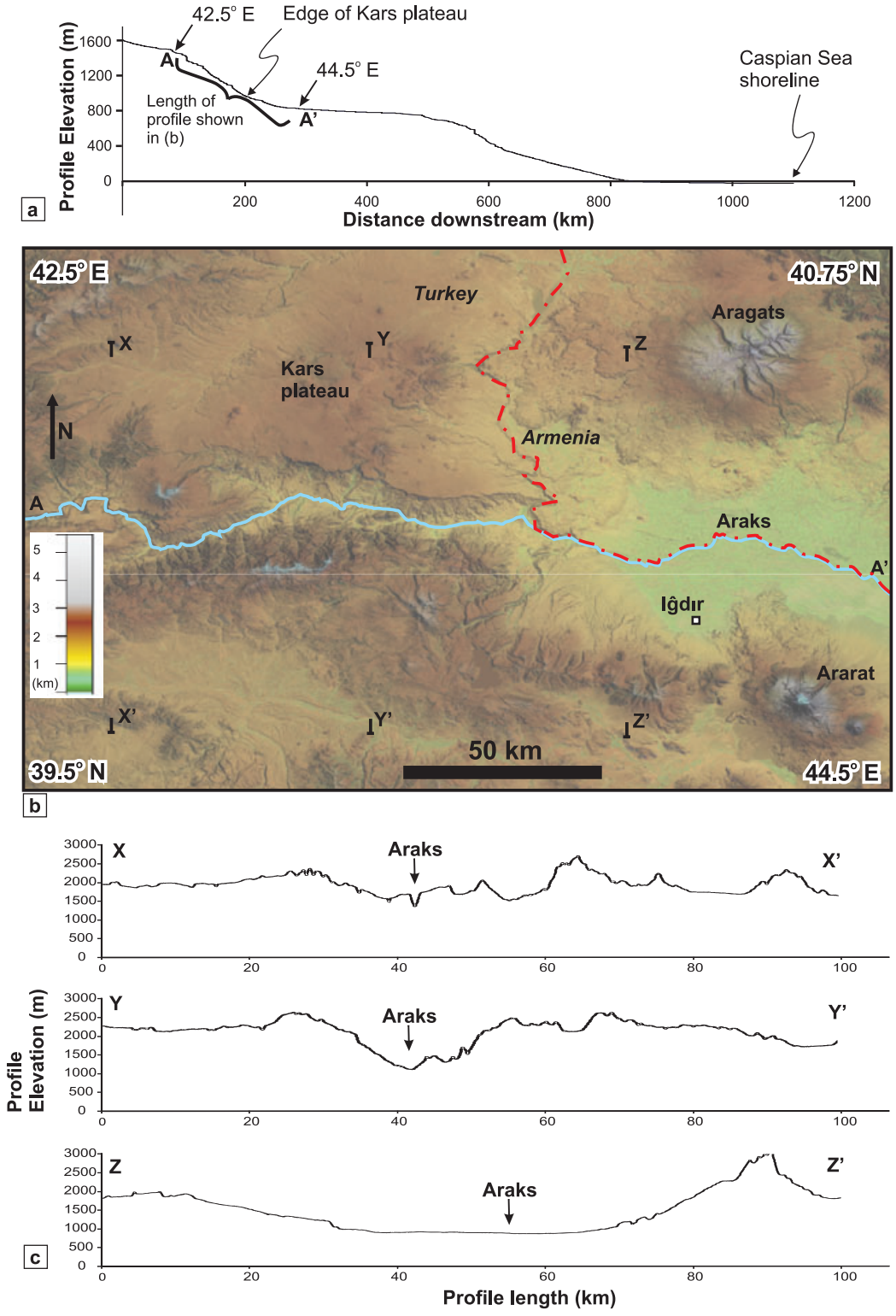

Figure 3. Geomorphology of the Araks River, Kars plateau and adjacent areas. (a) River long profile for the Araks, derived from SRTM data; (b) 50 per cent transparent Landsat 7 imagery draped over SRTM digital topography, in the region of the steep reach of the Araks, highlighted in part (a); (c) three cross-valley profiles of the Araks River, located on (b), showing the low relief, domal form of the Kars plateau on profiles X–X′ and Y–Y′.

the main drainage divide in the region (Fig. 2), which here separates rivers that flow east to Lake Urumieh (Fig. 1), and west to the Greater Zab, which joins the Tigris.

The Siah Cheshmeh pull-apart basin lies along the Gailatu-Siah Cheshmeh-Khoy Fault, which is an active northwest–southeast trending, right-lateral strike-slip system (Fig. 2, Karakhanian *et al.* 2004; Copley & Jackson 2006). This basin forms a local topographic depression in the ranges crossed by the Zang-e-Mar River. Both the Zang-e-Mar and rivers to its north and south pre-date the faulting, as they appear to be offset right-laterally by as much as

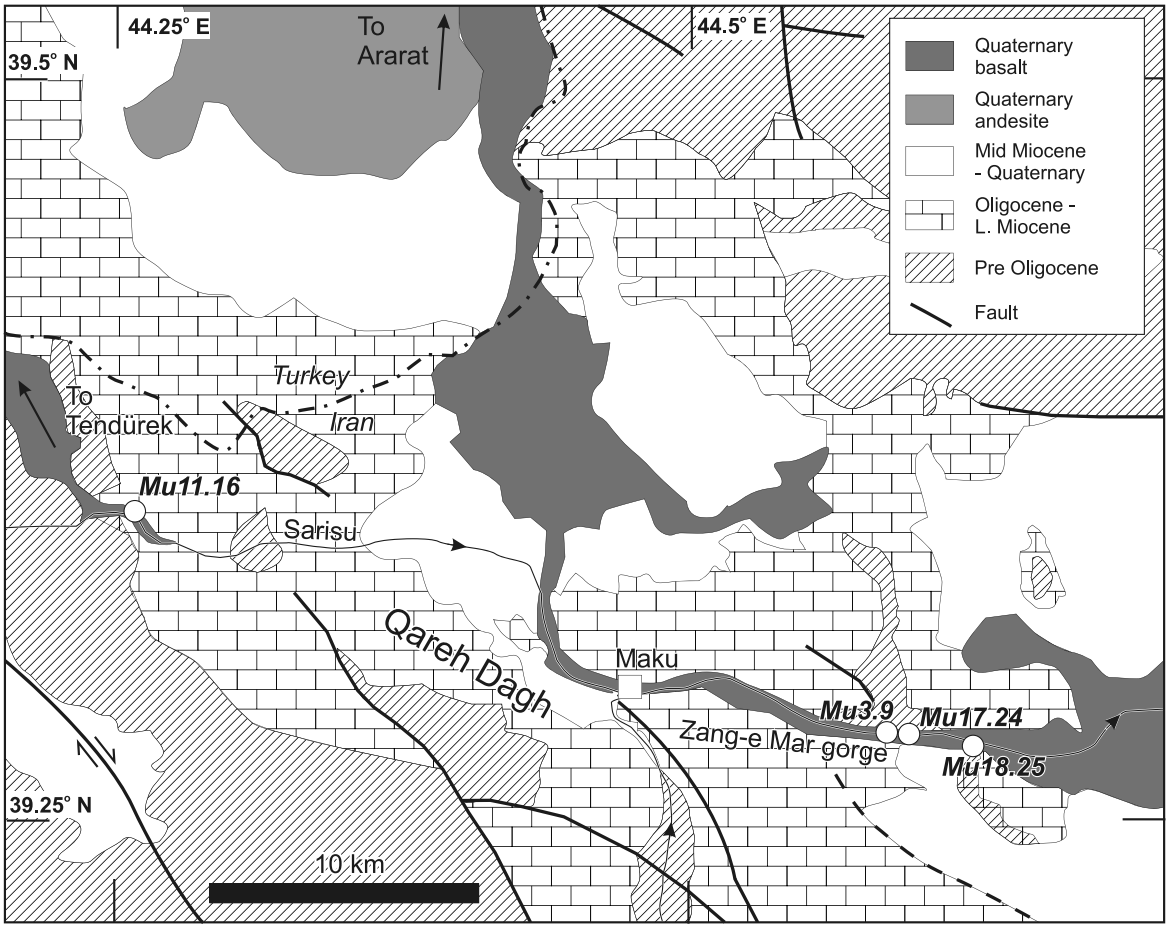

Figure 4. Geological map of the area around Maku, showing sample localities for four of the five samples dated in this study. Derived from Alavi & Bolourchi (1975) and Şenel (2002).

13 km (Copley & Jackson 2006), and maintain channels that cut across the topography on the eastern side of the Siah Cheshmeh pull-apart and smaller depressions at Kelisa Kandi and Qarehqush Pa'in (Fig. 2).

The Zang-e-Mar has other reaches where it shows its antecedent nature (Fig. 4). The first of these reaches is along a south–north gorge, 12 km long, through Permian and Oligocene–Miocene limestones of the Qareh Dagh range. The river then turns eastwards at Maku, where it enters an east–west gorge and runs for 14 km through the Oligocene–Miocene limestones, before entering a plain and joining the Araks. Other smaller regions also have low relief and elevations without the obvious structural control present at Siah Cheshmeh. These include the plains around Salmas and Khoy (Fig. 2), where the rivers are not incised in to the Quaternary deposits, indicating that the reaches are aggradational and the rivers are transport-limited rather than detachment-limited.

3 VALLEYS, GORGES AND LAVA FLOWS

3.1 Lava distribution

All analysed samples are from flows that covered tens of kilometres from Ararat, Tendürek or Yigit Dagi, lying within pre-existing river channels. This is not typical: most flows lie on or adjacent to the volcanic centres. Samples Mu3.9 and Mu17.24 are likely to be from the same flow from Ararat. Four of the lavas in this study come from the valleys and gorges cut by tributaries of the Araks (Figs 2 and 4): three are from the Zang-e-Mar (Mu3.9, Mu17.24 and Mu18.25; Figs 5a–d). At least two flows passed through the Zang-e-Mar, based on the presence of a flow top part way up the exposure. The fourth sample is from the Sarisu river, which joins the Zang-e-Mar at Maku (Mu11.16, Figs 5e–f). The fifth sample (Mu14.19) comes from the valley of the Rud-e Roshadeh, which flows into Lake Urumieh (Figs 1 and 2). Other lavas from similar settings were sampled close to the Rud-e Roshadeh, but yielded highly discordant age spectra, and have not been possible to date (not shown). In each sampled area there is a thin skim of alluvium and/or soil above the lava flow, implying little or no erosion of the regional surface since eruption, outside of the incised river channel.

3.2 Valley and gorge depths: methodology

Two methods were used to calculate gorge and valley depths for this study. In the field, a simple plumb line was lowered in to gorges and the depth measured. This is especially suitable for the narrowest gorges such as the Zang-e-Mar, where the gorge width is only on the order of a few metres (Figs 5a and b), cut in to the lavas. These gorges are not properly resolved on Shuttle Radar Topography Mission (SRTM) data, where the pixel size is 90 m.

Where wider and deeper valleys are present the depths and cross-section profiles are calculated from SRTM data (Jarvis *et al*. 2008). SRTM data have a specified vertical absolute accuracy of $\leq$16 m

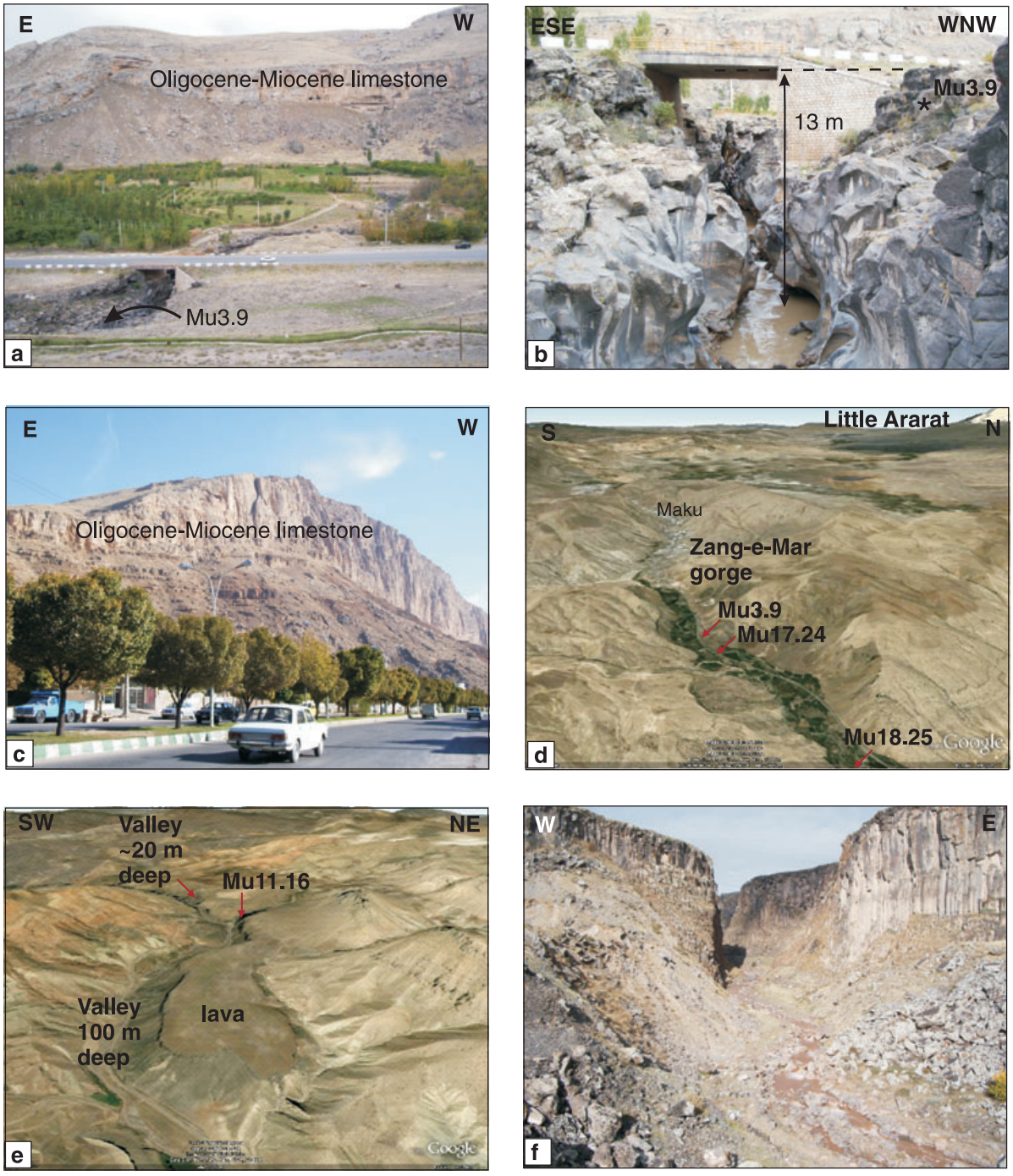

Figure 5. Landscape at sample localities for this study. (a) Zang-e-Mar gorge at sample locality Mu3.9; (b) view along slot gorge through lava, at sample locality Mu3.9; (c) general view of the Zang-e-Mar gorge at Maku; (d) oblique view along the Zang-e-Mar gorge (©Google Earth; ©2010 DigitalGlobe; ©2010Cnew/SPOT image); (e) oblique view along the Sarisu gorge, near Kelisa Kandi (©Google Earth; ©2010 DigitalGlobe; ©2010Cnew/SPOT image); (f) Sarisu gorge at sample locality Mu11.16.

(Rodriguez *et al.* 2005). Gorokhovich & Voustianiouk (2006) found it ranged from 7.58 ± 0.60 m to 4.07 ± 0.47 m in two local case studies. Specific vertical relative accuracy is quoted as ≤10 m (Rodriguez *et al.* 2005).

3.3 Valley and gorge depths: results

Gorge depths are in the range 5.7–25 m at the localities of the five dated samples (Table 1). These are isolated measurements of the fluvial incision since eruption at each locality, and do not fully describe the incision in to the lavas along the reaches containing the lava flows—that is, our spot measurements do not reflect how the incision varies upstream and downstream from our sample sites. Cross-valley topographic profiles derived from SRTM and plumb line data show that the amount of post-lava fluvial incision can vary greatly along a single valley. For example, local incision at the site of sample Mu11.16 in the Kelisa Kandi valley is 25 m, but 2 km to the east at the downstream limit of the flow it is 100 m (Figs 5e

Table 1. Summary of local fluvial incision in to lavas at sample localities, and maximum valley relief.

Sample	Local post-lava incision (m)	Maximum valley relief (m)
Mu3.9	13	750
Mu11.16	25	400
Mu14.19	25	520
Mu17.24	13	750
Mu18.25	5.7	750

and f). The river has cut right through the lava at the downstream section of the flow. The Rud-e Roshadeh shows a different pattern, where incision increases upstream of the sample site for Mu14.19 (local incision: 25 m), and downstream dies out as the river enters the plains around Salmas. Incision of the Zang-e-Mar gorge (Fig. 4) is greater within the gorge at Maku (13 m at sample sites Mu3.9 and Mu17.24, Fig. 5d) than to the west (9 m) and east (5.7 m at sample site Mu18.25, Fig. 5d).

On a bigger scale, the post-eruption relief in each valley/gorge system is only a small part of the total relief. Whereas incision into the lavas is on the scale of tens of metres, the overall valley profiles show relief on the scale of hundreds of metres, and typically in the range 300–500 m at the Zang-e-Mar and Kelisa Kandi sample sites (Figs 2 and 5d, Table 1).

4 ^{40}Ar/^{39}Ar DATING

4.1 Samples and methodology

All samples are basaltic, which is more basic than normal for these volcanoes, but consistent with the length of the flows, which implies low viscosities. Ararat samples are tholeiitic; the others are alkalic. Full geochemical descriptions of the samples are given in Kheirkhah *et al.* (2009). Detailed petrographic information is within Kheirkhah (2007). Trace element geochemical signatures include a negative Nb, Ta anomaly, indicative of either a source modified by subduction or contamination by a suitable source. Crustal contamination is evident in the Ararat samples, where indices such as Th/Yb show a positive correlation with SiO_2, but is not confirmed from the chemistry of the more basic samples from other centres. Nd and Sr isotopes suggest two different source end-members across the region, with Ararat tapping a more depleted source than the centres to its south.

For ^{40}Ar/^{39}Ar dating, visibly altered areas of basalt hand samples were removed using a slow-rotating saw. The sample was subsequently crushed in a jaw crusher to yield >500 μm fragments. A disc mill was used to produce a 250–500 μm separate. The sample was cleaned in distilled water to remove the fine fraction and subsequently sieved. A Frantz magnetic separator was used to remove phenocryst-bearing groundmass from grains of groundmass. The groundmass samples were subsequently leached in dilute nitric acid in an ultrasonic bath. The process was repeated six times until the acid remained clear. The groundmass was finally rinsed in distilled water and methanol in an ultrasonic bath. Approximately 500 mg of sample (phenocryst-free groundmass) was picked by hand under a binocular microscope for dating.

Samples were loaded into Cu foil packets and positioned within quartz vials for irradiation. Adjacent to each sample packet we placed Al-foil wrapped packets of the international standard Alder Creek sanidine (1.193 $\pm$ 0.001 Ma, Nomade *et al.* 2005) to permit characterization of the irradiation flux to the samples. Fish Canyon Tuff sanidine (FC-2s, 28.02 $\pm$ 0.56 Ma, Renne *et al.* 1998) was loaded into the same vials to check J-parameter consistency. The sample was irradiated in the McMaster reactor for 1 hr in the Cd-lined facility. Interference correction factors and J-values are presented in the online Supporting Information.

^{40}Ar/^{39}Ar ages were determined at the NERC Argon Isotope Facility, which is housed at the Scottish Universities Environmental Research Centre. Samples were step-heated from 500–1750 °C using an all-metal resistance furnace. Extracted gases were cleaned by a combination of cold finger (maintained at –95.5 °C by a slush trap) and three GP50 getters (two maintained at 450 °C and one at room temperature). Following 5 min of heating the extracted gases were cleaned for 10 min. An ARGUS multicollector noble gas mass spectrometer was used to collect Ar isotope data (Mark *et al.* 2009). ARGUS has a measured sensitivity of 7×10^{-14} moles per volt. Hot furnace blanks were run immediately prior to conducting all experiments. A set of 10 air calibrations were run pre- and post-experiment to monitor mass discrimination.

The Berkeley Geochronology Centre software *MassSpec* was used to regress and reduce age data. Isotope data are corrected for blank, radioactive decay, mass discrimination and interfering reactions. ^{40}Ar/^{39}Ar ages also include uncertainties to the J-parameter from analyses of 30 standard crystals per bracketing J-packet. The parameters of Steiger & Jäger (1977) were used for calculation of ages.

4.2 Results

The raw ^{40}Ar/^{39}Ar data are located in the Supporting Information. Fig. 6 shows the ^{40}Ar/^{39}Ar step-heating spectra and isotope correlation plots (inverse isochrones) for all samples. Table 2 provides a summary of all sample ages and defines plateau criteria. All ^{40}Ar/^{39}Ar ages and uncertainties are quoted at the 1σ level. We discuss each sample below:

Mu18.25 (Ararat): The sample yielded steps with low radiogenic argon (^{40}Ar*, typically 10–20 per cent) signals and as such the uncertainties associated with age calculation are relatively large. The age spectrum shows a plateau age of 0.81 $\pm$ 0.10 Ma. The inverse isochron shows no excess argon ($^{40}Ar_E$) with the trapped composition overlapping accepted air values (^{40}Ar/^{36}Ar = 295.5 $\pm$ 0.5, Nier 1950). The plateau, inverse isochron and integrated age all overlap at 2σ levels showing the ^{40}Ar/^{39}Ar age data to be robust.

Mu17.24 (Ararat): Again low ^{40}Ar* yields are responsible for relatively imprecise ages. The age spectrum yields an age of 0.40 $\pm$ 0.05 Ma. The inverse isochron overlaps with the accepted air values at the 2σ level (Nier 1950) and yields a similar ^{40}Ar/^{39}Ar age to the age spectrum. The age spectrum, inverse isochron and integrated age all overlap at the 1σ levels showing the ^{40}Ar/^{39}Ar age data to be robust.

Mu3.9 (Ararat): Once again, relatively low ^{40}Ar* yields produce relatively large uncertainties in ^{40}Ar/^{39}Ar ages. The age spectrum yields a plateau age of 0.48 $\pm$ 0.03 Ma. The inverse isochron shows that the trapped component overlaps with accepted air values (Nier 1950) and gives a similar age to the plateau age. The plateau, inverse isochron and integrated age all overlap showing the ^{40}Ar/^{39}Ar data to be robust.

Mu11.16 (Tendürek): This sample has higher ^{40}Ar* yields (20–60 per cent ^{40}Ar*) than previous samples (reflected by the lower uncertainty in ^{40}Ar/^{39}Ar ages). The age spectrum yields a plateau age of 0.49 $\pm$ 0.01 Ma. The inverse isochron shows that the trapped

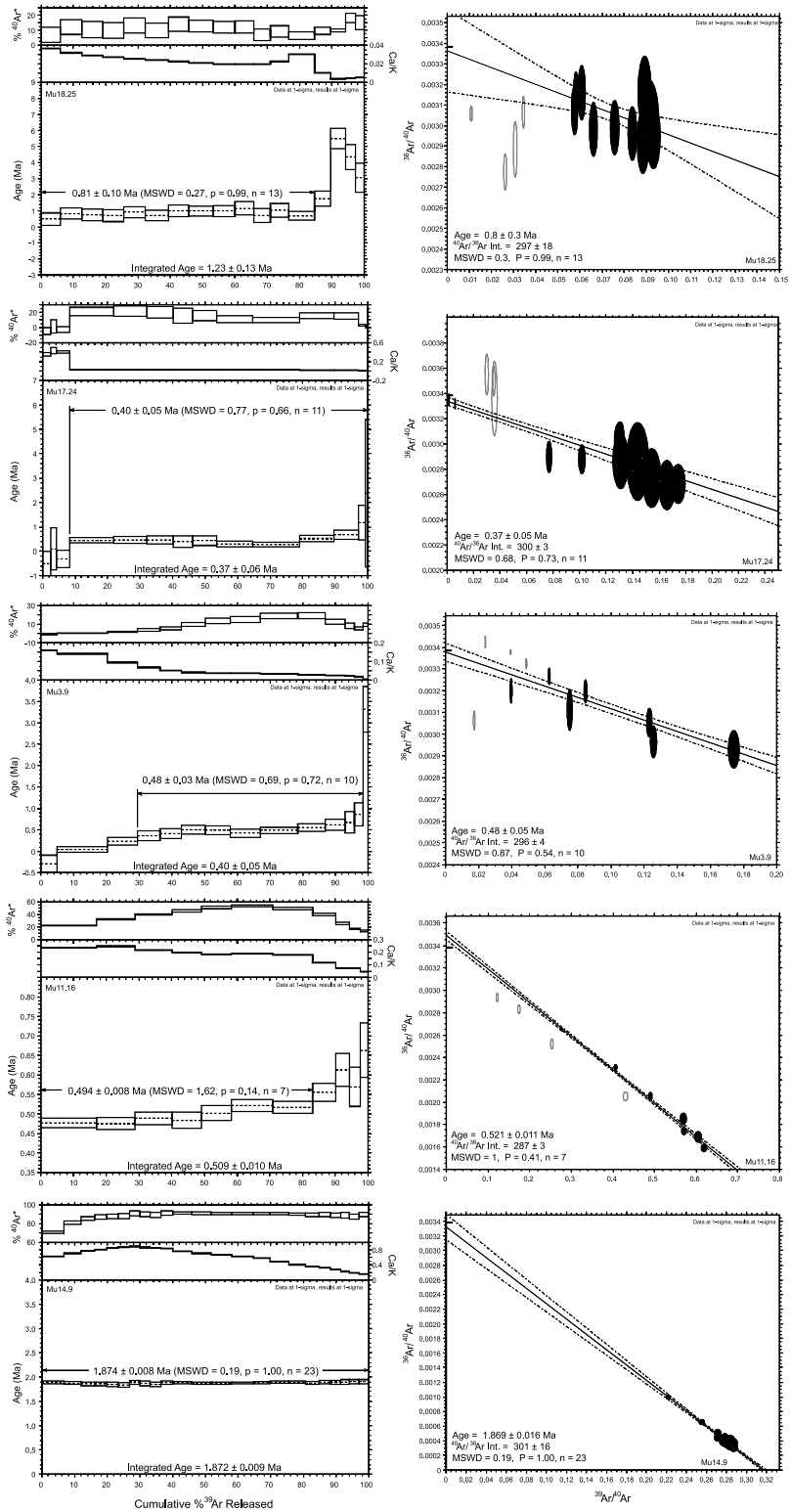

Figure 6. Age spectra (left-hand side) and inverse isochrons (right-hand side) for all samples. The integrated $^{40}Ar/^{39}Ar$ age is also presented on the age spectra. Black ellipses shown in the inverse isochron are accepted data whereas grey ellipses show rejected data.

component overlaps with accepted air values (Nier 1950). The rejected steps in the inverse isochron plot show the presence of $^{40}Ar_E$ in the high temperatures. The plateau and integrated $^{40}Ar/^{39}Ar$ ages overlap at 1σ but these only overlap with the inverse isochron $^{40}Ar/^{39}Ar$ age at 2σ levels. We consider the plateau age to be robust.

Mu14.19 (Yigit Dagi): The age spectrum is completely concordant yielding relatively high $^{40}Ar^*$ signals (70–90 per cent). The age provided by the plateau calculation is 1.87 ± 0.01 Ma. The inverse isochron shows that all the data plot relatively close to the $^{39}Ar/^{40}Ar$ axis giving an age of 1.869 ± 0.016 Ma. The $^{40}Ar/^{36}Ar$ component

Table 2. Summary of $^{40}Ar/^{39}Ar$ data including mass of material analysed.

Sample #	Mass of sample step-heated (mg)	$^{40}Ar/^{39}Ar$ plateau age (Ma)	±1s (Ma)	^{39}Ar (per cent)	*n*	Inverse isochron $^{40}Ar/^{39}Ar$ age (Ma)	±1s (Ma)	$^{40}Ar/^{39}Ar$	±1s ±1s	Integrated age (Ma)	±1s (Ma)
Mu18.25	472	0.81	0.10	84	13	0.80	0.30	297	18	1.23	0.13
Mu17.24	550	0.40	0.05	92	11	0.37	0.05	300	3	0.37	0.06
Mu3.9	566	0.48	0.03	69	10	0.48	0.05	296	4	0.40	0.05
Mu11.6	440	0.49	0.01	83	7	0.52	0.01	296	4	0.51	0.01
Mu14.9	520	1.87	0.01	100	23	1.87	0.02	301	16	1.87	0.01

overlaps with accepted air values (Nier 1950). The plateau, inverse isochron and integrated age all overlap showing the data to be robust.

Table 2 shows the plateau, inverse isochron and integrated ages for all samples. Throughout this manuscript when discussing sample age we will cite the $^{40}Ar/^{39}Ar$ age provided by the plateau calculations for all samples.

5 DISCUSSION

5.1 Volcanic chronology

The Quaternary ages obtained in this study are consistent with previously published K-Ar ages for the Ararat and Tendürek volcanic centres (Pearce *et al.* 1990; Yilmaz *et al.* 1998). Published Ararat ages range from 1.5 to 0.1 Ma, so that the ages for the samples in this study (0.4, 0.48 and 0.81 Ma) are well within this range. Sample Mu18.25 is older than the other two samples from the Zang-e-Mar gorge, suggesting that at least two flows passed through this valley (and consistent with fieldwork observations). Published Tendürek ages fall between 0.7 and 0.013 Ma—which bracket the 0.49 Ma age for sample Mu11.16. Neither centre has a well-documented pre-Quaternary history (Yilmaz *et al.* 1998), although this cannot be ruled out given that the oldest flows are likely to be concealed beneath younger ones. Flows from Yigit Dagi have not previously been dated, so that the 1.87 Ma age determined for sample Mu14.19 is a first age for this centre. It is older than the flows from Ararat and Tendürek analysed in this and other studies, which is consistent with its more subdued morphology. While Ararat and Tendürek can be considered as dormant, Yigit Dagi seems to be extinct.

5.2 Incision and landscape evolution

The main purpose of this study was to date the lava flows that exploited the regional drainage, to get a better idea of the incision rates and landscape evolution of the region before and during the volcanic phase.

Post-eruption incision rates at the sample sites are on the order of 0.01–0.05 mm yr^{-1}, calculated by dividing the local gorge depth by the age of the lava (Table 3). Incision rates are lowest to the east of the Zang-e-Mar gorge (0.01 mm yr^{-1}) and at the Rud-e-Roshadeh (0.01 mm yr^{-1}), and higher within the Zang-e-Mar gorge (0.03 mm yr^{-1}) and along the Kelisa Kandi valley (0.05 mm yr^{-1}).

Table 3. Post-lava fluvial incision rates at each sample locality.

Sample	Post-lava incision rate (mm yr^{-1})
Mu3.9	0.03
Mu11.16	0.05
Mu14.19	0.01
Mu17.24	0.03
Mu18.25	0.01

As noted in Section 3.3, it is clear that incision varies considerably along each river valley where lava is present. One reason for this is shown in Fig. 7, which illustrates how a lava flow generates relief at the end of the flow. When drainage re-establishes itself, there is a knickpoint at this location, which will migrate upstream over time. Variations in incision will be present along the river channel until the river has re-equilibrated. This is seen in the Kelisa Kandi valley, where incision decreases upstream along the river valley from the present lower limit of the lava flow (Fig. 5f). The incision in to the lava is therefore higher than it would be in an equivalent valley without a lava flow, making the incision rates maximum values for local fluvial incision in the Quaternary.

Incision in to the lava along the Zang-e-Mar is lower at either end of the gorge than within it (5.7–9 m, vs. 13 m). There are two possibilities here. One is that the lava part-filled and ponded within the gorge, such that a knickpoint was generated at the eastern end of the gorge that has migrated upstream (there is no evidence for this, however). The second is that the spur of the Qareh Dagh has undergone faster surface uplift than adjacent areas, generating greater river incision along it. These are not mutually exclusive explanations. Incision along the Rud-e Roshadeh decreases eastwards where it enters the plains around Salmas, similar to the situation east of the Zang-e-Mar gorge, but is more pronounced as the river eventually ceases to incise and is instead filling the surrounding basin with alluvium before entering Lake Urumieh.

There is also the issue that the original lava flow surfaces need not have been smooth and parallel to the initial and present valley floors. However, we discount this from being a significant factor, given the low-viscosity nature of the flows and the lack of evidence for such relief within the gorges or adjacent plains.

Therefore the fluvial incision rates presented here cannot simply be extrapolated to give regional incision rates, but imply that Quaternary incision has been a relatively slow process, that is, only tens of metres in a million years. This inference is reinforced when the regional landscape is considered. The gorges that are cut in to the lavas represent only a small fraction of the total relief in each valley, in the order of <5 per cent (Table 1). The present day cross-valley profile in Fig. 8a shows that the post-lava gorges represent an even smaller proportion of the total material eroded from each valley. It is not possible to calculate exactly the regional relief within this part of the plateau before the eruptions, but it is unlikely that it was significantly greater than at present: this would require the removal of material from the hillslopes at a rate faster than the fluvial incision in the valley floors. Another factor is lithology: the basaltic flows may be more resistant to erosion than the country rock. However, the limestone at the Zang-e-Mar gorge and elsewhere is mechanically strong and capable of forming cliffs (Fig. 5c). Therefore we deduce that it is unlikely that the lava lithology has significantly skewed the overall pattern of incision and erosion.

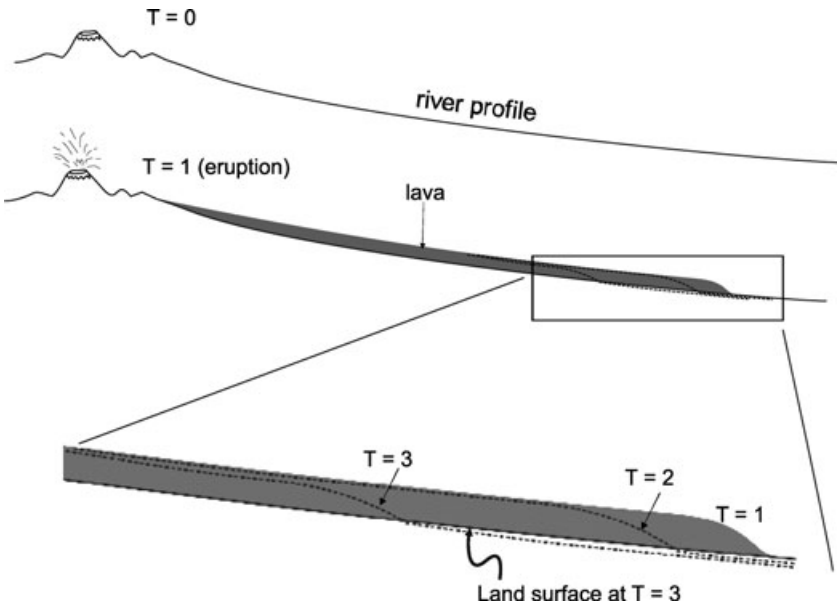

Figure 7. Schematic topographic evolution along a river profile before and after the eruption of a lava at time $T = 1$. Inset diagram shows knickpoint migration upstream of the lava termination at times $T = 2$ and $T = 3$, illustrating how local post-lava incision varies along the length of the flow.

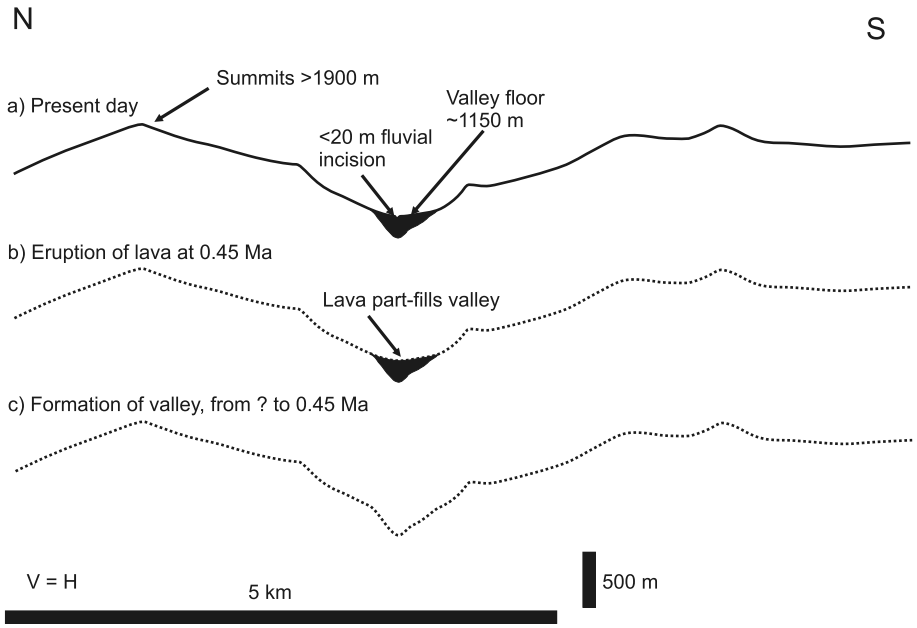

Figure 8. Topographic evolution in northwest Iran, using a cross-valley profile for the Zang-e-Mar (Fig. 2) and the average age of samples Mu3.9 and Mu17.24 as examples. (a) Present day topography (from SRTM data), total lava thickness is not constrained, but incision is <20 m; (b) topography at the time of eruption, 0.45 Ma, with little difference in summit elevations or overall relief compared with present day; (c) topography just before eruption at 0.45 Ma is therefore similar to present landscape.

We conclude that the greater part of the relief in the Maku region (∼1 km) pre-dates the Quaternary lava flows, and that the eruptive phase has not been associated with any acceleration of relief or incision (Fig. 8). Given the likely 10–20 Myr timescale of compressional deformation within the Turkish–Iranian plateau, the Quaternary rates could apply on longer timescales to produce the overall relief.

Similarly, there is no simple relationship between surface uplift rate and river incision rate, but in graded rivers the faster the former, the faster the latter is expected to be, given that rivers respond to an increase in gradient with an increase in stream power and hence erosive capability. Complications can arise for various reasons, including the local perturbation to the river long profile represent by the lava flow itself, as described. On a regional scale there is potentially a time lag between the surface uplift and the geomorphic response. For transport-limited systems this may be very rapid, with effectively uniform incision onset throughout the drainage basin (Whipple & Tucker 2002). In detachment-limited systems, the incision pulse and knickpoint migration move vertically upstream at a rate equivalent to the surface uplift rate (Niemann *et al.* 2001). The rivers in northwest Iran have alternating incising and aggrading reaches. It is therefore possible that they have not

yet fully responded to any Quaternary regional surface uplift. It is therefore useful to look for a wave of incision downstream of the study area which might be the signal of Quaternary regional surface uplift: the Araks River has higher gradients for ∼100 km at the junction of the Lesser Caucasus and Talysh ranges, compared with upstream or downstream, but this is exactly the place where such gradients would be expected as the river leaves the Turkish–Iranian plateau (Figs 1 and 3). We propose that like the relief generation, surface uplift is also likely to have been as slow during the Quaternary volcanic phase as pre-Quaternary times, but do not completely rule it out, if the knickzone at the Lesser Caucasus/Talysh junction turns out to be related to an upstream-propagating wave of incision.

These results have wider implications for the tectonics of northwest Iran and the Turkish–Iranian plateau, and the origin of the late Cenozoic plateau magmatism. Both the slab break-off and lower lithosphere delamination models have been reported elsewhere in the world and/or modelled as associated with major surface uplift (England & Houseman 1988; Buiter *et al.* 2002; Andrews & Billen 2009) at rates of mm yr^{-1} (e.g. Westaway 1993). Our findings suggest that if either process has occurred beneath the plateau in northwest Iran, it is not associated with major generation of relief, at least in the Quaternary. We favour Late Cenozoic compressional tectonics as the most likely explanation for the generation of relief and elevations in our study area. The lack of Quaternary folding and thrusting is consistent with low relief generation during the volcanic phase.

The surface uplift history of the entire Turkish–Iranian plateau need not be homogeneous. Radiometric age data are emerging from the Turkish sector of the plateau and the adjacent Arabian Platform for Quaternary volcanics in this region, which suggest marked variations in the pattern of landscape evolution (Demir *et al.* 2007a,b; Seyrek *et al.* 2008; Demir *et al.* 2009; Westaway *et al.* 2009), including at least local rapid surface uplift (e.g. Seyrek *et al.* 2008), and a domal component to the topography of east Anatolia (Şengör *et al.* 2003). The geomorphology along the Araks upstream of our study area supports such ideas of a low relief, domal uplift within east Anatolia, with a long wavelength knickzone developed along a ∼1 km deep valley through the Kars plateau, where regional topography slopes gently eastwards (Figs 3a and b). This area has steeper slopes at lower elevations, below low relief highlands (Fig. 3c; profiles X–X′ and Y–Y′). Our results from northwest Iran indicate a more prosaic pattern of landscape evolution, without rapid Quaternary incision and/or uniform surface uplift. Therefore there may be two separate patterns of landscape development, with different causes, within the Turkish–Iranian plateau in eastern Turkey and northwest Iran.

6 CONCLUSIONS

The geology of the extreme northwest tip of Iran includes lava flows from three composite volcanoes that passed down pre-existing river valleys. New $^{40}Ar/^{39}Ar$ ages of these lavas are Quaternary, ranging from 1.87 to 0.4 Ma. Fluvial incision in to these lavas is no more than a few tens of metres, indicating Quaternary fluvial incision rates on the order of 0.01–0.05 mm yr^{-1}. Given that regional relief is on the scale of hundreds of metres (Figs 2 and 7, Table 1), we conclude that the Quaternary is not a time of rapid erosion, relief generation or surface uplift in northwest Iran. However, this pattern of landscape evolution contrasts with the adjacent area in eastern Anatolia, where the volcanics originated, and where a broad domal uplift is associated with the main centres for late Cenozoic magmatism. It is this pattern of magmatism, and its underlying cause, which likely holds the key to the landscape evolution in eastern Anatolia, whereas in northwest Iran relief generation is largely controlled by compressional tectonics that pre-date the magmatism in this area.

ACKNOWLEDGMENTS

We are grateful to the Geological Survey of Iran for their support. NERC are thanked for continued funding of the Argon Isotope Facility at the Scottish Universities Environmental Research Centre (SUERC), which is funded by the Scottish Universities consortium. R. Dymock and J. Imlach (SUERC) are thanked for technical assistance. The $^{40}Ar/^{39}Ar$ work was funded by NIGFSC grant IP/980/0507. MBA and MK are grateful to the Royal Society for travel support. We acknowledge productive discussions with Alex Densmore and Paolo Ballato. James Jackson produced the epicentre files used in Fig. 1. Two anonymous referees provided very helpful comments.

REFERENCES

Ahmadzadeh, G., Jahangiri, A., Lentz, D. & Mojtahedi, M., 2010. Petrogenesis of Plio-Quaternary post-collisional ultrapotassic volcanism in NW of Marand, NW Iran, *J. Asian Earth Sci.,* **39,** 37–50.

Alavi, M. & Bolourchi, M., 1975. Geological Quadrangle Map of Iran, 1:250,000 scale, sheet A1 (Maku), Geol. Surv. Iran.

Allen, M., Jackson, J. & Walker, R., 2004. Late Cenozoic reorganization of the Arabia-Eurasia collision and the comparison of short-term and long-term deformation rates., *Tectonics,* **23,** TC2008, doi:10.1029/2003TC001530.

Allen, M.B. & Armstrong, H.A., 2008. Arabia-Eurasia collision and the forcing of mid Cenozoic global cooling, *Palaeogeogr., Palaeoclimatol., Palaeoecol.,* **265,** 52–58.

Allen, M.B., Kheirkhah, M., Emami, M.H. & Jones, S.J., 2011. Right-lateral shear across Iran and kinematic change in the Arabia–Eurasia collision zone, *Geophys. J. Int.,* **184,** 555–574, doi:10.1111/j.1365-246X.2010.04874.x.

Andrews, E.R. & Billen, M.I., 2009. Rheologic controls on the dynamics of slab detachment, *Tectonophysics,* **464,** 60–69.

Angus, D.A., Wilson, D.C., Sandvol, E. & Ni, J.F., 2006. Lithospheric structure of the Arabian and Eurasian collision zone in eastern Turkey from S-wave receiver functions, *Geophys. J. Int.,* **166,** 1335–1346.

Ballato, P., Uba, C.E., Landgraf, A., Strecker, M.R., Masafumi, S., Stockli, D.F., Friedrich, A. & Tabatabaei, S.H., 2011. Arabia-Eurasia continental collision: insights from late Tertiary foreland-basin evolution in the Alborz mountains, northern Iran, *Bull. Geol. Soc. Am.,* **123,** 106–131, doi:10.1130/B3009.1.

Buiter, S.J.H., Govers, R. & Wortel, M.J.R., 2002. Two-dimensional simulations of surface deformation caused by slab detachment, *Tectonophysics,* **354**, 195–210.

Copley, A. & Jackson, J., 2006. Active tectonics of the Turkish-Iranian Plateau, *Tectonics,* **25,** TC6006, doi:10.1029/2005TC001096.

Davidson, J., Hassanzadeh, J., Berzins, R., Stockli, D.F., Bashukooh, B., Turrin, B. & Pandamouz, A., 2004. The geology of Damavand volcano, Alborz Mountains, northern Iran, *Bull. Geol. Soc. Am.,* **116,** 16–29.

Demir, T., Westaway, R., Bridgland, D., Pringle, M., Yurtmen, S., Beck, A. & Rowbotham, G., 2007a. Ar-Ar dating of late Cenozoic basaltic volcanism in northern Syria: implications for the history of incision by the River Euphrates and uplift of the northern Arabian Platform, *Tectonics,* **26,** TC3012, doi:10.1029/2006tc001959.

Demir, T., Westaway, R., Bridgland, D.R. & Seyrek, A., 2007b. Terrace staircases of the River Euphrates in southeast Turkey, northern Syria and western Iraq: evidence for regional surface uplift, *Quat. Sci. Rev.* **26,** 2844–2863.

Demir, T., Seyrek, A., Guillou, H., Scaillet, S., Westaway, R. & Bridgland, D., 2009. Preservation by basalt of a staircase of latest Pliocene terraces of the River Murat in eastern Turkey: evidence for rapid uplift of the eastern Anatolian Plateau, *Glob. Planet. Change,* **68,** 254–269.

Dewey, J.F., Hempton, M.R., Kidd, W.S.F., Saroglu, F. & Şengör, A.M.C., 1986. Shortening of continental lithosphere: the neotectonics of Eastern Anatolia: a young collision zone, *Geol. Soc. Lond. Spec. Pub.,* **19,** 3–36.

England, P.C. & Houseman, G.A., 1988. The mechanics of the Tibetan plateau, *Phil. Trans. R. Soc. London,* **326,** 301–319.

Gorokhovich, Y. & Voustianiouk, A., 2006. Accuracy assessment of the processed SRTM-based elevation data by CGIAR using field data from USA and Thailand and its relation to the terrain characteristics, *Remote Sens. Environ.,* **104,** 409–415.

Hatzfeld, D. & Molnar, P., 2010. Comparisons of the kinematics and deep structures of the Zagros and Himalaya and of the Iranian and Tibetan plateaus and geodynamic implications, *Rev. Geophys.,* **48,** RG2005, doi:10.1029/2009rg000304.

van Hunen, J. & Allen, M.B., 2011. Continental collision and slab break-off: a comparison of 3-D numerical models with observations. *Earth planet. Sci. Lett.,* **302,** 27–37, doi:10.1016/j.epsl.2010.11.035.

Jackson, J., 2001. Living with earthquakes: know your faults, *J. earthq. Eng.,* **5,** 5–123.

Jackson, J., Haines, A.J. & Holt, W.E., 1995. The accommodation of Arabia-Eurasia plate convergence in Iran, *J. geophys. Res.,* **100,** 15 205–15 209.

Jarvis, A., Reuter, H.I., Nelson, A. & Guevara, E., 2008. Hole-filled SRTM for the globe, Version 4. Available from the CGIAR-CSI SRTM 90m Database; http://srtm.csi.cgiar.org (last accessed 2001 January 20).

Karakhanian, A.S. *et al*., 2004. Active faulting and natural hazards in Armenia, eastern Turkey and northwestern Iran, *Tectonophysics,* **380,** 189–219.

Keskin, M., 2003. Magma generation by slab steepening and breakoff beneath a subduction-accretion complex: an alternative model for collision-related volcanism in Eastern Anatolia, Turkey, *Geophys. Res. Lett.,* **30,** 1–4.

Keskin, M., Pearce, J.A. & Mitchell, J.G., 1998. Volcano-stratigraphy and geochemistry of collision-related volcanism on the Erzurum-Kars Plateau, northeastern Turkey, *J. Volc. Geotherm. Res.,* **85,** 355–404.

Keskin, M., Pearce, J.A., Kempton, P.D. & Greenwood, P., 2006. Magma-crust interactions and magma plumbing in a postcollisional setting: geochemical evidence from the Erzurum-Kars volcanic plateau, eastern Turkey, *Spec. Pub. Geol. Soc. Am.,* **409,** 475–505.

Kheirkhah, M., 2007. The Petrology and Geochemiscal studies on Quaternary basaltic rocks in NW of Iran (Azerbaijan), *PhD thesis*, Azad University, Tehran.

Kheirkhah, M., Allen, M.B. & Emami, M., 2009. Quaternary syn-collision magmatism from the Iran/Turkey borderlands, *J. Volc. Geotherm. Res,* **182,** 1–12.

Lebedev, V.A., Sharkov, E.V., Keskin, M. & Oyan, V., 2010. Geochronology of Late Cenozoic volcanism in the area of Van Lake, Turkey: an example of development dynamics for magmatic processes, *Dokl. Earth Sci.,* **433,** 1031–1037.

Lustrino, M., Keskin, M., Mattioli, M., Lebedev, V.A., Chugaev, A., Sharkov, E. & Kavak, O., 2010. Early activity of the largest Cenozoic shield volcano in the circum-Mediterranean area: Mt. Karacadag, SE Turkey, *Eur. J. Mineral.,* **22,** 343–362.

Maggi, A. & Priestley, K., 2005. Surface waveform tomography of the Turkish-Iranian plateau, *Geophys. J. Int.,* **160,** 1068–1080.

Mark, D.F., Barfod, D., Stuart, F.M. & Imlach, J., 2009. The ARGUS multi-collector noble gas mass spectrometer: performance for $^{40}Ar/^{39}Ar$ geochronology, *Geochem. Geophys. Geosys.,* **10,** 1525–2027.

Molnar, P., Boos, W.R. & Battisti, D.S., 2010. Orographic controls on climate and paleoclimate of Asia: Thermal and mechanical roles for the Tibetan Plateau, *Ann. Rev. Earth and Planet. Sci.,* **38,** 77–102.

Morley, C.K. *et al*., 2009. Structural development of a major late Cenozoic basin and transpressional belt in central Iran: the Central Basin in the Qom-Saveh area, *Geosphere,* **5,** 325–362.

Niemann, J.D., Gasparini, N.M., Tucker, G.E. & Bras, R.L., 2001. A quantitative evaluation of Playfair's law and its use in testing long-term stream erosion models, *Earth Surf. Process. Landf.,* **26,** 1317–1332.

Nier, A.O., 1950. A redetermination of the relative abundances of the isotopes of carbon, nitrogen, oxygen, argon, and potassium, *Phys. Rev.,* **77,** 789–793.

Nomade, S., Renne, P.R., Vogel, N., Deino, A.L., Sharp, W.D., Becker, T.A., Jaouni, A.R. & Mundil, R., 2003. Alder Creek sanidine (ACs-2): a Quaternary $^{40}Ar/^{39}Ar$ dating standard tied to the Cobb Mountain geomagnetic event, *Chem. Geol.,* **218,** 315–338.

Okay, A.I., Zattin, M. & Cavazza, W., 2010. Apatite fission-track data for the Miocene Arabia-Eurasia collision, *Geology,* **38,** 35–38.

Parlak, O., Delaloye, M., Demirkol, C. & Unlugenc, U.C., 2001. Geochemistry of Pliocene/Pleistocene basalts along the Central Anatolian Fault Zone (CAFZ), Turkey, *Geodinamica Acta,* **14,** 159–167.

Paul, A., Hatzfeld, D., Kaviani, A., Tatar, M. & Péquegnat, C., 2010. Seismic imaging of the lithospheric structure of the Zagros mountain belt (Iran), *Geol. Soc. Lond. Spec. Pub.,* **330,** 5–18.

Pearce, J.A. *et al*., 1990. Genesis of collision volcanism in eastern Anatolia, Turkey, *J. Volc. Geotherm. Res,* **44,** 189–229.

Priestley, K. & McKenzie, D., 2006. The thermal structure of the lithosphere from shear wave velocities, *Earth. planet. Sci. Lett.,* **244,** 285–301.

Radjaee, A., Rham, D., Mokhtari, M., Tatar, M., Priestley, K. & Hatzfeld, D., 2010. Variation of Moho depth in the central part of the Alborz Mountains, northern Iran, *Geophys. J. Int.,* **181,** 173–184.

Raymo, M.E., Ruddiman, W.F. & Froelich, P.N., 1988. Influence of Late Cenozoic mountain building on ocean geochemical cycles, *Geology,* **16,** 649–653.

Reilinger, R. *et al*., 2006. GPS constraints on continental deformation in the Africa-Arabia-Eurasia continental collision zone and implications for the dynamics of plate interactions, *J. geophys. Res.,* **111,** B05411, doi:10.1029/2005JB004051.

Renne, P.R., Swisher, C.C., Deino, A.L., Karner, D.B., Owens, T.L. & DePaolo, D.J., 1998. Intercalibration of standards, absolute ages and uncertainties in $^{40}Ar/^{39}Ar$ dating, *Chem. Geol.,* **145,** 117–152.

Reuter, M. *et al*., 2009. The Oligo-/Miocene Qom Formation (Iran): evidence for an early Burdigalian restriction of the Tethyan Seaway and closure of its Iranian gateways, *Int. J. Earth Sci.,* **98,** 627–650.

Ritz, J.F., Nazari, H., Ghassemi, A., Salamati, R., Shafei, A., Solaymani, S. & Vernant, P., 2006. Active transtension inside central Alborz: a new insight into northern Iran-southern Caspian geodynamics, *Geology,* **34,** 477–480.

Rodriguez, E., Morris, C.S., Belz, J.E., Chapin, E.C., Martin, J.M., Daffer, W. & Hensley, S., 2005. An assessment of the SRTM topographic products, Jet Propulsion Laboratory, Pasadena, California. Technical Report D-31639, 1–143.

Schildgen, T.F., Hodges, K.V., Whipple, K.X., Reiners, P.W., & Pringle, M.S., 2007. Uplift of the western margin of the Andean plateau revealed from canyon incision history, southern Peru, *Geology,* **35,** 523–526.

Sella, G.F., Dixon, T.H. & Mao, A., 2002. REVEL: a model for recent plate velocities from space geodesy, *J. geophys. Res.,* **107,** 2081, doi:10.1029/2000JB000033.

Şenel, M., 2002. *Geological Map of Turkey, 1:500,000 Sale,* General Directorate of Mineral Research and Exploration, Ankara.

Şengör, A.M.C., Ozeren, S., Genc, T. & Zor, E., 2003. East Anatolian high plateau as a mantle-supported, north-south shortened domal structure, *Geophys. Res. Lett.,* **30,** 8045, doi:10.1029/2003GL017858.

Şengör, A.M.C., Ozeren, M.S., Keskin, M., Sakinc, M., Ozbakir, A.D. & Kayan, I., 2008. Eastern Turkish high plateau as a small Turkic-type orogen: implications for post-collisional crust-forming processes in Turkic-type orogens, *Earth-Sci., Rev.,* **90,** 1–48.

Seyrek, A., Demir, T., Pringle, M., Yurtmen, S., Westaway, R., Bridgland, D., Beck, A. & Rowbotham, G., 2008. Late Cenozoic uplift of the Amanos Mountains and incision of the Middle Ceyhan river gorge, southern Turkey: Ar-Ar dating of the Duzici basalt, *Geomorphology,* **97,** 321–355.

Shabanian, E., Bellier, O., Siame, L., Arnaud, N., Abbassi, M.R. & Cocheme, J.J., 2009. New tectonic configuration in NE Iran: active strike-slip faulting between the Kopeh Dagh and Binalud mountains, *Tectonics,* **28,** TC5002, doi:10.1029/2008tc002444.

Steiger, R.H., & Jäger, E., 1977. Subcommission on geochronology: convention on the use of decay constants in geo- and cosmochronology, *Earth planet. Sci. Lett.,* **36,** 359–362.

Taghizadeh-Farahmand, F., Sodoudi, F., Afsari, N. & Ghassemi, M.R., 2010. Lithospheric structure of NW Iran from P and S receiver functions, *J. Seismol.,* **14,** 823–836.

Valla, P.G., Herman, F., Van Der Beek, P.A. & Braun, J., 2010. Inversion of thermochronological age-elevation profiles to extract independent estimates of denudation and relief history, I: theory and conceptual model, *Earth. planet. Sci. Lett.,* **295,** 511–522.

Van Der Beek, P.A., Valla, P.G., Herman, F., Braun, J., Persano, C., Dobson, K.J. & Labrin, E., 2010. Inversion of thermochronological age-elevation profiles to extract independent estimates of denudation and relief history, II: application to the French Western Alps, *Earth. planet. Sci. Lett.,* **296,** 9–22.

Vernant, P. *et al*., 2004. Contemporary crustal deformation and plate kinematics in Middle East constrained by GPS measurements in Iran and northern Iran, *Geophys. J. Int.,* **157,** 381–398.

Walker, R.T., Gans, P., Allen, M.B., Jackson, J., Khatib, M., Marsh, N. & Zarrinkoub, M., 2009. Late Cenozoic volcanism and rates of active faulting in eastern Iran, *Geophys. J. Int.,* **177,** 783–805.

Westaway, R., 1993. Quaternary uplift of southern Italy, *J. Geophys. Res.,* **98**, 21741–21772.

Westaway, R., Guillou, H., Seyrek, A., Demir, T., Bridgland, D., Scaillet, S. & Beck, A., 2009. Late Cenozoic surface uplift, basaltic volcanism, and incision by the River Tigris around Diyarbakir, SE Turkey, *Int. J. Earth Sci.,* **98,** 601–625.

Whipple, K.X. & Tucker, G.E., 2002. Implications of sediment-flux-dependent river incision models for landscape evolution, *J. geophys. Res.,* **107,** 2039, doi:10.1029/2000JB000044.

Yilmaz, Y., Guner, Y. & Saroglu, F., 1998. Geology of the quaternary volcanic centres of the east Anatolia, *J. Volc. Geotherm. Res,* **85,** 173–210.

Zor, E., Sandvol, E., Gürbüz, C., Türkelli, N., Seber, D. & Barazangi, M., 2003. The crustal structure of the East Anatolian plateau from receiver functions, *Geophys. Res. Lett.,* **30,** 8044, doi:10.1029/2003GL018192.

SUPPORTING INFORMATION

Additional Supporting Information may be found in the online version of this article:

Supplement S1. Details of $^{40}Ar/^{39}Ar$ analyses.

Please note: Wiley-Blackwell are not responsible for the content or functionality of any supporting materials supplied by the authors. Any queries (other than missing material) should be directed to the corresponding author for the article.